Batteries & Supercaps

Research Article
doi.org/10.1002/batt.202300140

**Chemistry
Europe**
European Chemical
Societies Publishing

www.batteries-supercaps.org

An Incremental Capacity Analysis-based State-of-health Estimation Model for Lithium-ion Batteries in High-power Applications

Hamid Hamed,[a, b] Marwan Yusuf,[d] Marek Suliga,[d] Behnam Ghalami Choobar,[a, b] Ryan Kostos,[d] and Mohammadhosein Safari*[a, b, c]

The Incremental Capacity (IC) is a rich source of data for the state-of-health estimation of lithium-ion batteries. This data is typically collected during a low C-rate (dis)charge of the battery which is not representative of many real-world applications outside the research laboratories. Here, this limitation is showcased to be mitigated by employing a new feature-extraction technique applied to a large dataset including 105 batteries with cycle lives ranging from 158 to 1637 cycles. The state-of-health of these batteries is successfully predicted with a mean-absolute-percentage error below 0.7 % by using three regression models of support vector regressor, multi-layer perceptron, and random forest. The methodologies proposed in this work facilitate the development of accurate IC-based state-of-health predictors for lithium-ion batteries in on-board applications.

Introduction

Accurate state-of-health (SoH) prediction of the lithium-ion batteries (LIBs) is a very desired functionality for the battery management systems (BMS) to ensure a safe and optimal control of battery-powered devices such as electric vehicles.[1] Equivalent circuit models (ECMs),[2] physics-based models[1,2] and pure data-driven methods have been extensively proposed and investigated in the literature to predict the SoH of LIBs.[3] Although the ECM-based models have the privilege of being implemented online, they normally fail to predict the nonlinear aging behavior, what is known as accelerated aging zone or "knee-point".[4] This shortcoming can be avoided in the physics-based models,[1] but at the expense of longer computational times[5] and the need for a prior knowledge about the active aging mechanisms. The pure data-driven models and machine-learning (ML) approaches are emerging as a promising alternative to predict the SoH of batteries.[6] In this category,

the Neural networks (NNs) and support vector machines have been successfully employed to predict battery SOH and remaining useful life (RUL) using three time-dependent data streams which are obtained during the life of a battery, i.e., current, voltage, and temperature.[6,7] More recently, 'feature engineering' has been employed by the data-driven models in which transformations of the raw data are used as the input to the models also known as health indicators (HIs). A widely studied class of HIs is based on the incremental capacity (IC) and differential voltage (DV) analysis.[8] The value of the peaks/valleys, the position of the peaks/valleys and peak/valley area in the IC/DV curves have shown significant correlation with the battery SOH and RUL.[8c,9] This highlights the importance of the hidden information of the voltage data which has shown higher predictability of the SoH compared to the battery capacity or internal resistance that are extensively studied as conventional HIs.[10] For instance, Severson et al.[17] showed that the changes between the voltage curve of very early cycles can accurately classify the cells into the relatively short and long life cells.

The technique of differential analysis has been widely used to study various Lithium-Ion Battery (LIB) chemistries, such as LFP, NMC, and LTO.[11] Typically, these studies focus on investigating aging data obtained from low-rate constant-current experiments. Jiang et al.[12] conducted research on large-format LFP cells and analyzed their incremental capacity (IC) curves. They discovered that the main cause of degradation was the loss of lithium inventory and anode material. Additionally, they demonstrated that by using features extracted from the IC curve peaks, a prediction accuracy up to 97 % for SoH could be achieved. Ansean et al.[13] conducted a thorough IC peak area analysis on LFP|Gr chemistry to create look-up tables that can be used to identify aging modes, with the aim of simplifying the implementation of the differential analysis method in the battery management systems. Li et al.[8c] utilized

a combination of incremental capacity method and Gaussian process regression to analyze a part of the NASA aging dataset. Their results demonstrated highly accurate SoH prediction mean absolute error (MAE) and root mean square error (RMSE) being less than 1%. Tang et al.[14] conducted a study on various aging data repositories that are publicly available, including the NASA and SONY aging datasets. In order to predict the SoH, they extracted features from the peak position and peak value of the filtered IC curves, which they referred to as regional capacity and regional voltage. The method they used resulted in an estimation error of 2.5% for all the batteries that were studied. Lu et al.[15] suggested a two-stage method to estimate the SoH of LFP/Gr cells by examining the degradation modes and implementing a deepCoral-based domain adaptation technique. Their approach was successfully validated with both synthetic and real aging data from seven cells and resulted in accurate SoH predictions. An efficient way to enlarge the sample size data is to use physics-based models to generate synthetic aging data. Costa et al.[16] utilized a convolutional neural network (CNN) in order to investigate a substantial synthetic aging dataset which consisted of over 700,000 representative C/25 charge cycles for LFP, NMC, and NCA. They implemented Dynamic Time Warping to convert the IC curves into images, which were subsequently utilized as the CNN's input. This method yielded more impressive outcomes compared to the state-of-the-art methods, with an average RMSPE error of roughly 2% for 1000 duty cycles. Another option is to analyze existing large experimental aging datasets to train reliable and accurate models. For instance, Severson et al.[17] conducted an experiment with 124 LFP|Gr cells with an aging period of approximately two years. Kheirkhah et al.[18] utilized this dataset and applied various regression learners, selecting input features based on charging and discharging time. They reported a MAPE error of 1.95% for the SoH prediction. Moreover, Ma et al.[19] conducted aging tests on 77 LFP|Gr cells, each cell subjected to a unique discharge protocol, while all the cells were charged using an identical fast-charging protocol. They employed a deep transfer learning technique and utilized the information of the preceding 30 cycles to estimate capacity at a given time. Their approach led to a mean testing error of less than 0.2%. One advantage of their approach is its ability to accommodate vastly different load protocols and generalize the model to forecast new, unseen load protocols.

In this paper, a data-driven SoH prediction model is proposed by extending the application of ICA to the cells cycled at high discharge rates. This is important since real-world battery data are in general characterized by a rather high C-rate which degrades the data quality extracted from the numerical differentiation of the voltage-capacity raw data being the basis of IC/DV techniques. In this regard, a novel feature extraction method is developed based on a pattern recognition algorithm to analyze the discharge IC curves. The methodology is then applied to a large aging data repository provided by Severson et al.[17] After extracting the features, three distinct regression models namely Support Vector Regressor (SVR), Random Forest (RF), and Multi-Layer Percep-

tron (MLP) are trained and validated demonstrating a high level of accuracy in estimating the SoH of 105 cells with LFP|Graphite chemistry.

Results and Discussions

Feature extraction from aging dataset

Here, the experimental dataset generated by Severson et al.[17] is used to train and develop 3 different models of Support Vector Regressor (SVR), Random Forest (RF), and Multi-Layer Perceptron (MLP) for SoH prediction (see supporting information). The dataset investigated in the present study covers the charge/discharge behavior of 105 high-power LFP|Graphite A123 APR18650M1A cells cycled with a constant current-constant voltage (CC-CV) protocol. The cells were fast charged using different profiles, but all were discharged with the same CC-CV profile at 4 C with 2.0 V and of C/50 as the cut-off voltage and current, respectively. The charging profile consisted of one-step or two-step charging periods from 0% to 80% state of charge (SOC) and thereafter up to 100% SOC using a 1 C CC-CV step with 3.6 V and C/50 as the cut-off voltage and current, respectively. The lifetime of the cells varies between 158 to 1637 cycles with the end of life defined as the 20% capacity loss relative to the nominal capacity of the pristine cells (Figure 1). The SoH at a given time 't_i' is defined as the ratio of the available capacity at time 't_i' relative to the capacity at the beginning of life ($t_i = 0$).

The features used for SoH estimation are based on the incremental capacity analysis (ICA). In a conventional ICA, the battery charge throughput (Ah) is recorded using the Coulomb counting method during a charge or discharge process at a very low current. The most significant information can be extracted from the IC curves from pseudo-equilibrium conditions, i.e., C-rates in the range of C/20 or lower.[20] The IC plots are obtained by differentiating the capacity (Q) vs. voltage (V) curves with respect to the voltage ($\frac{dQ}{dV}$) and are characterized by the presence of peaks. The peak positions in the $\frac{dQ}{dV}$ vs. V plots and the areas under such peaks are very sensitive to the cell parameters including but not limited to the redox potentials of the Li-insertion particles in the anode and cathode, cell balancing, and the internal resistance.[21] Any change in these parameters during the lifetime of the cell will be reflected as a deviation in the IC signature of the cell relative to that of the cell at its beginning of life.

At high C-rates, the peaks in the IC curves start to merge, and the features that differentiate them become indistinguishable. Although IC curve peak positions are effective in estimating SoH, they are very sensitive to the noise. To overcome these shortcomings, here, an iterative search algorithm is proposed that calculates the difference between the IC curves of the fresh cell at the beginning of life (BoL) and that of the aged cell at a given time. The algorithm is based on the image registration, an image processing technique used to align multiple scenes into a single integrated image.[22] Similarly, the algorithm of the present study aligns the two IC
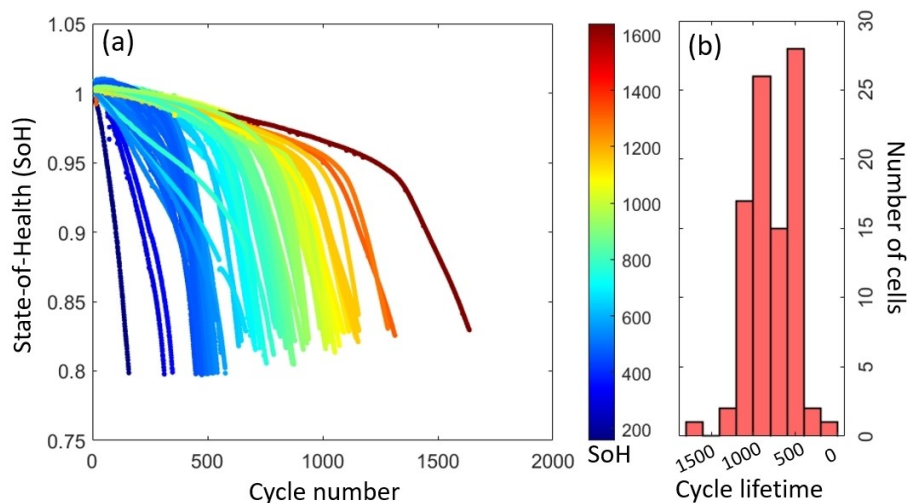
Batteries & Supercaps

Research Article
doi.org/10.1002/batt.202300140

Chemistry Europe
European Chemical
Societies Publishing

Figure 1. a) SoH as a function of cycle number for the 105 cells (LFP│Graphite A123)[17] studied in this work. The color bar encodes the life cycle of the cells. b) The distribution of the cycle lives of the cells.

curves to quantify the scaling of the IC plot induced by aging in both the voltage and incremental capacity dimensions (Figure S1). The as obtained two scaling factors, i.e., IC-scale and V-scale, are the features to train the data-driven models. This feature extraction method involves comparing the IC curve of the nth cycle to that of the BOL and adjusting the two scales until the difference between the two curves is minimized (Figure 2a and b, see Supporting Information for more details).

This feature extraction method resulted in a matrix of features comprising of two columns, namely V-scale and IC-scale, and 78438 rows that correspond to the cycle lives of the 105 cells analyzed. The V-scale and IC-scale values are shown against their corresponding SoH values in Figures 2(c) and (d), respectively. The Pearson correlation coefficients of 0.86 and 0.96 among the SOH and the Vscale and IC-scale, respectively,
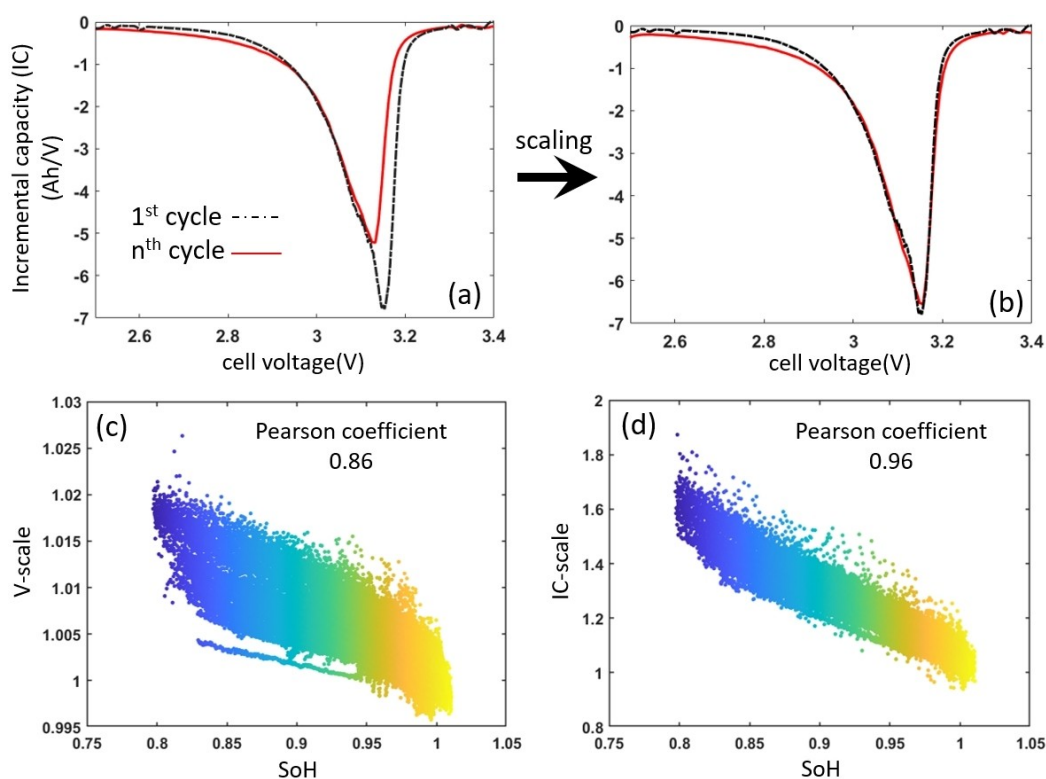

Figure 2. A typical scaling of the IC plot a) at a given cycle (n^{th} cycle) with respect to the beginning of life (cycle #1) to extract the two features of V-scale and IC-scale, b) by matching the IC plots of the 1st and n^{th} cycle. The correlation between the resulted features and State of Health (SoH), showing a strong correlation among c) the V-scale and SoH and d) IC-scale and SoH. The colors encode the SoH with blue representing a lower SoH.

Batteries & Supercaps

Research Article
doi.org/10.1002/batt.202300140

Chemistry Europe

European Chemical
Societies Publishing

indicate the high predictive power of these features for the SoH (Figure 2c and d).

Parametrization of the SoH models

The dataset was randomly split into two categories of 'train-validation' (60%) and 'test' cells (40%). The train-validation dataset was further randomly grouped into two categories of 'training' (60%) and 'validation' (40%) (see SI for more details). First, the hyperparameters for the three regression models of SVR, MLP, and RF were optimized by exploring a range of model parameters using the 'train-validation' cells. To achieve this, the model was trained on the train dataset for each combination of model parameters. Once the training was complete, the model was tested on the validation dataset. The model parameters that resulted in the lowest prediction error on the validation dataset were selected as the final model parameters. The optimized model parameters are summarized in Table 1 (block I). The prediction accuracy of the three regression models is compared in terms of the RMSE and MAPE errors in Table 1 (block II). A comparison between the performance of the three models show that all of them work well in fitting the training dataset with RMSE of around 0.01 and MAPE of less than 1%. However, the RF model slightly outperforms the other two models which is also reflected in its higher R^2 score value. The residual value, defined as the difference between the predicted SoH and the actual SoH using the training dataset is shown as a function of the actual SoH for the SVR model in Figure 3(a) and for the MLP and RF models in Figure S2. The data show that for all the three models, the residuals are scattered randomly around zero and do not show any particular pattern as a function of the target variable, i.e., actual SoH, indicating that all the three models can be considered as a proper fit to the training datasets.

Validation of the SoH models

To further validate our results, the regression models were again trained with the "train-validation" dataset while preserving the same hyperparameters from the previous training step (Table 1, block I). The performance of the regression models after this new round of training is presented in Figure for the five randomly selected cells (for each model) from the "train-validation" dataset. Overall, all three models show satisfactory results in predicting the SoH. The predicted SoH values from the MLP model, however, show a higher deviation from the actual SoH compared to the outputs of RF and SVR models. This is in line with the higher MAPE and RMSE errors associated with MLP model (Table 1).

Next, the newly trained models (i.e., trained on "train-validation" datasets) were applied to the test dataset. The resulting RMSE, MAPE and model scores are presented in Table 1 (block III). The predicted SoH values by SVR and RF models are compared against the actual SoH values in Figure 4 for the three cells that showed the lowest estimation error (Figure and 4 C) and three cells that had the highest estimation errors (Figure and 4d). Although both SVR and RF models show extremely accurate predictions for most of the representative cells, there are certain cells (Figure 4) of which the predicted SoHs display a noticeable deviation from the actual SoH values. This might be linked to the unique behavior of this certain group of the cells with an increasing capacity during the first few cycles which deserves further attention in the following works. However, despite the large errors for this group of cells, it is noteworthy that the models still do a good job in predicting the overall aging trajectory and particularly the accelerated aging phase of the cells (Figure 4b and d). This is, in particular important for the identification of the so-called knee point in SoH diagnosis and prognosis models.

The method proposed in this study works very well on the IC curves obtained from 4 C discharge data. The versatility of

Table 1. The optimized regression models' parameters (I block) obtained after training the models by the 'train + validation' dataset and the corresponding RMSE, MAPE and goodness of fit (R^2) values when the model was applied on the 'validation' dataset (II block). SoH prediction accuracy of the models trained by the 'train + validation' and applied on 'test' dataset (III block) and '50multiples' (IV block) datasets.

I. Optimized parameters of the regression models with 'train + validation' dataset			II. model metrics trained with 'validation' dataset		
			RMSE	MAPE%	R^2
SVR	$C = 1374$ $\varepsilon = 0.01$ $\gamma = 1.79$		0.0108	0.88	0.943
MLP	$\alpha = 0.001$ Hidden layer size $= (50,50)$		0.0116	0.86	0.935
RF	Max depth $= 10$ Min samples leaf $= 4$ Min samples split $= 10$		0.0104	0.712	0.946
	validation phase				

III. Validation of model trained by 'train + validation' dataset against 'test' dataset			IV. Validation of model trained by '50multiple' dataset against 'test' dataset.		
	RMSE	MAPE%	R^2	RMSE	MAPE%	R^2
SVR	0.0102	0.75	0.945	0.0096	0.74	0.945
MLP	0.0109	0.815	0.938			
RF	0.0104	0.72	0.943	0.014	0.89	0.904

RMSE formula
$$RMSE = \left(\frac{1}{N} \sum_{i=1}^{N} \left(SoH_{pred} - SoH_{actual} \right)^2 \right)^{0.5}$$

MAPE formula
$$MAPE\% = \frac{100}{N} \sum_{i=1}^{N} \left| \frac{SoH_{pred} - SoH_{actual}}{SoH_{actual}} \right|$$
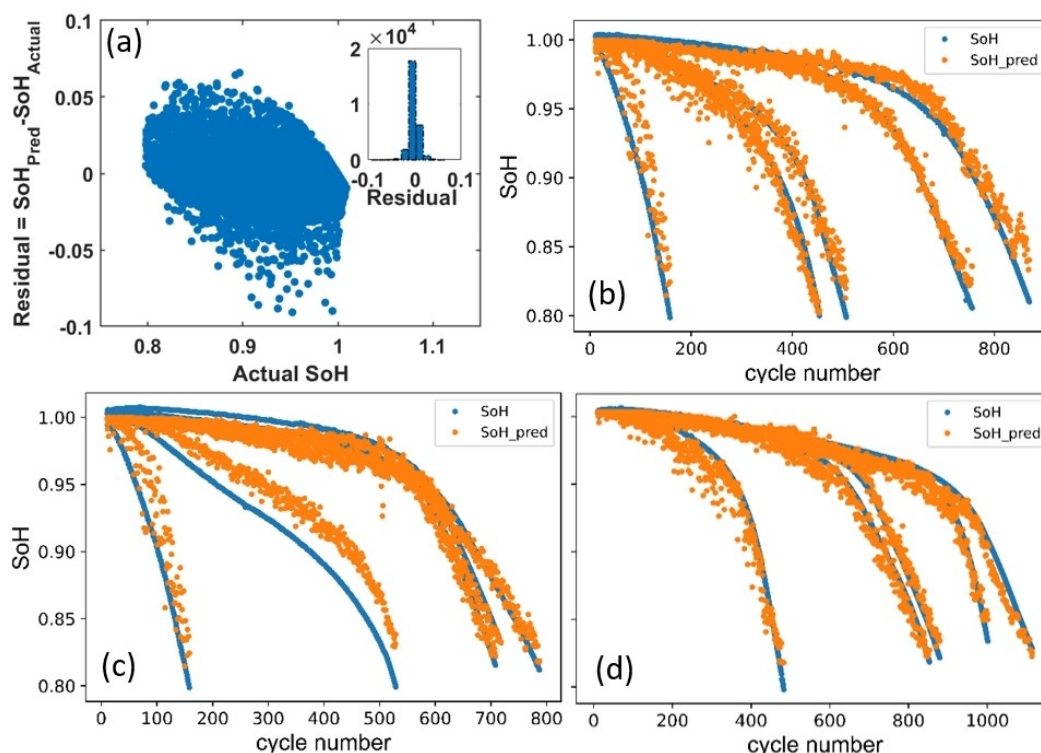
Figure 3. a)The residual, defined as the difference between the predicted SoH and actual SoH values, as a function of actual SoH using the 'training' dataset and SVR regression model. The figure inset shows the distribution of the residual following a symmetric distribution around zero. b–d) A visual guide into the predictive performance of the b) SVR, c) MLP and, d) RF regression models. The predicted SoH values are compared to the actual SoH values during the whole life of five randomly selected batteries from the 'train-validation' dataset.

this method was further investigated by training the regressor models using only a subset of the entire dataset ('50multiples'). This data subset includes the cycle numbers which are multiples of 50 to train the RF and SVR models of which the performance metrics are summarized in Table 1 (block IV). The results of the SVR model suggest that reliable SoH predictions can be achieved even when the training is performed with a limited portion of the entire dataset. This finding is particularly significant for real-world applications where frequent intermediate capacity checks may not be feasible or practical. A

comparison between the predicted and actual SoH values using the SVR and RF regression models on this subset of dataset are shown in Figure 5. Table 2 provides a summary of the state-of-the-art estimation models for SoH based on IC analysis reported in the literature for LFP|Gr cells. An unequivocal comparison among the different reports is not easy since the measure index of accuracy is not the same in different reports. Nonetheless, the prediction accuracy of the models proposed in the present study stand very competitive to the state-of-the-art with a MAPE < 0.75%. Noteworthy is the study of Zhou et al.[23]

Table 2. The scope and accuracy of the most recent data-driven SoH estimation models based on the IC analysis for the LFP|Graphite cells. It is important to note that the C-rate in this table refers the C-rate used for the IC analyses and does not correspond to the load profile applied during the battery aging.

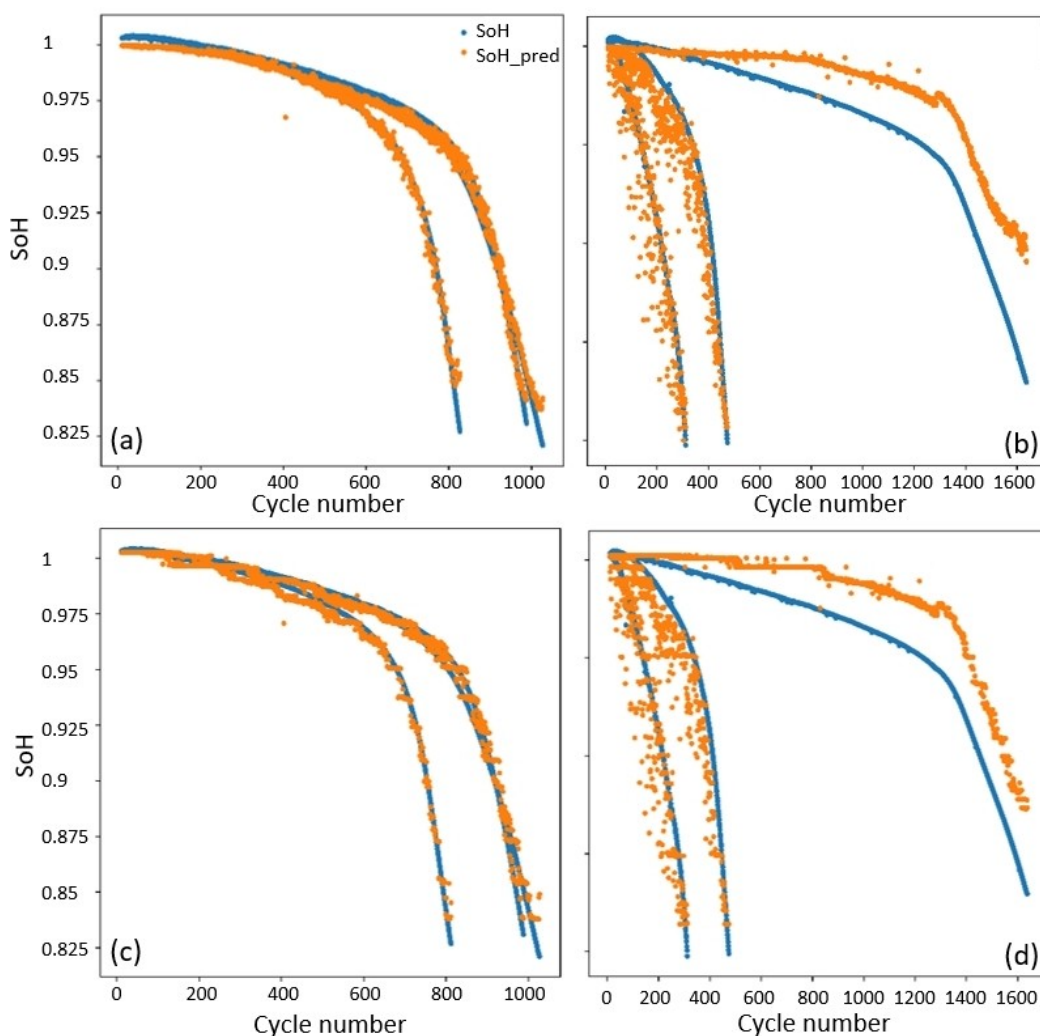| Health indicator	Battery chemistry (Capacity)	#batteries studied	C-rate	Evaluation index	Estimated precision	Ref.
IC curve (peak intensity)	LFP|Graphite (1.1 Ah)	8	0.5 C	Absolute error	1%	[8b]
Area under IC curve	LFP|Graphite (60 Ah)	4	0.33 C	Relative error	2%	[24]
IC curve (peak intensity)	LFP|Graphite (1.1 Ah)	30	0.5 C	RMSE	1.62%	[25]
IC curve (peak and valley)	LFP|Graphite (5 Ah)	2	1 C	Maximum relative error	4%	[9a]
IC curve (peak intensity and area under IC curve)	LFP|Graphite (20 Ah)	12	0.33 C	RMSE	0.9–2.1%	[11]
Area under the IC curve	LFP|Graphite (1.1 Ah)	35	Up to 4 C	MAPE	0.3309%	[23]
Area under IC curve	LFP|Graphite (50 Ah)	6	0.1 C	RMSE	3%	[12]

Figure 4. The predicted SoH as a function of cycle number for the three cells (test dataset) with a–c) the minimum estimation error and b–d) for the three cells with the maximum estimation error using a, b) the support vector machine regressor and c, d) random forest regressor.
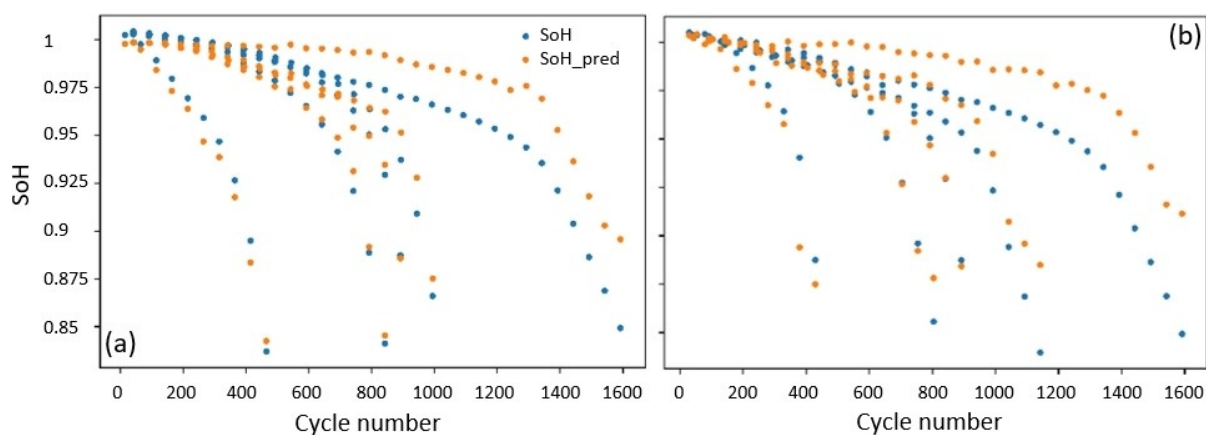

Figure 5. A visual guide into the accuracy of the SoH prediction models trained by the '50multiple' dataset, i.e., only cycle numbers multiples of 50, a) SVR and b) RF regression models. Predictions are compared against five randomly selected batteries from the 'test' dataset.

reporting a better MAPE of 0.3309% developed from a substantially smaller dataset of 35 cells compared to the present study, i.e., 105 cells. The size of the training and validation datasets is an extra important consideration which
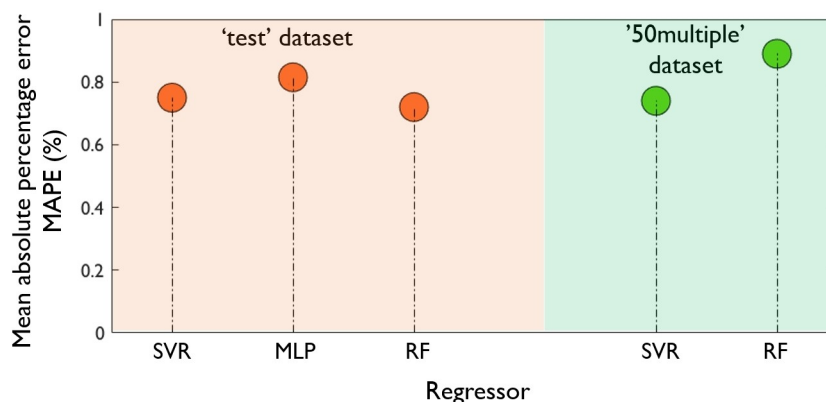
Batteries & Supercaps

Research Article
doi.org/10.1002/batt.202300140

Chemistry Europe
European Chemical
Societies Publishing

Figure 6. Performance comparison of the SVR, MLP, and RF regression models proposed in this study for the SOH prediction of the LFP|Graphite cells validated using the 'test' dataset (left compartment, brown) and the '50multiple' dataset (right compartment, green).

impacts the reliability of the model predictions for the field applications.

The accuracy of the three regression models validated on the 'test' and '50multiple' datasets is summarized in Figure 6. The SVR and RF models outperform the MLP model. The inferior accuracy of the MLP regressor might be explained by the fact that the MLP models typically require a relatively larger dataset to attain a high accuracy.[26] As such the present dataset might not be sufficient for the MLP to capture the underlying patterns and relationships as good as the SVR and RF models. Although the SVR and RF models exhibited similar performance on the original dataset, SVR outperforms RF on the '50multiple' dataset. It seems that on the '50multiple' dataset, the RF model encounters an overfitting problem reducing its accuracy in predicting the target variable. The RF's inferior accuracy on the smaller '50multiple' dataset suggests that the performance of this model, compared to the SVR model, is more sensitive to the size of the dataset.

Conclusions

In this study, differential capacity analysis method was applied to high-rate (4 C) discharge cycling data of 105 LFP\Gr cells with cycle lives ranging from 158 to 1637 cycles. A pattern recognition algorithm was used to juxtapose the differential capacity curves of each cycle to that of the first cycle. The searching algorithm resulted in two features, i.e., a scale of voltage and a scale to the incremental capacity. These features were then used by three different regressors to find suitable learners with the maximum prediction capabilities. Random forest regressor and support vector machines with radial basis kernel were found to yield MAPE errors below 1% for the prediction of SoH both on the test and validation datasets.

The findings of this work suggest that the differential analysis technique is not limited to low-rate charge and discharge cycling data and can be applied to very high C-rate data relevant to the on-board applications. This enables the development of short-lasting intermediate checkup protocols with a low frequency. Further improvements are needed to

extend the application of the proposed methodology of this work to the circumstances with an arbitrary partial charge and discharge protocols.

Supporting Information

Supporting Information is available from the Wiley Online Library or from the author.

Conflict of Interests

The authors declare that there is no conflict of interest.

Data Availability Statement

The data that support the findings of this study are available on reasonable request from the corresponding author.

[1] V. Sulzer, P. Mohtat, A. Aitio, S. Lee, Y. T. Yeh, F. Steinbacher, M. U. Khan, J. W. Lee, J. B. Siegel, A. G. Stefanopoulou, *Joule* **2021**, *5*, 1934–1955.
[2] H. Tian, P. Qin, K. Li, Z. Zhao, *J. Cleaner Prod.* **2020**, *261*, 120813.
[3] R. Xiong, L. Li, J. Tian, *J. Power Sources* **2018**, *405*, 18–29.
[4] S. Atalay, M. Sheikh, A. Mariani, Y. Merla, E. Bower, W. D. Widanage, *J. Power Sources* **2020**, *478*, 229026.
[5] J. Christensen, J. Newman, *J. Electrochem. Soc.* **2004**, *151*, A1977.
[6] Y. Li, K. Liu, A. M. Foley, A. Zülke, M. Berecibar, E. Nanini-Maury, J. Van Mierlo, H. E. Hoster, *Renewable Sustainable Energy Rev.* **2019**, *113*, 109254.

Batteries & Supercaps

Research Article
doi.org/10.1002/batt.202300140

Chemistry Europe
European Chemical
Societies Publishing

[7] L. Yao, S. Xu, A. Tang, F. Zhou, J. Hou, Y. Xiao, Z. Fu, *World Electric Vehicle J.* **2021**, *12*, 113.

[8] a) L. Zheng, J. Zhu, D. D.-C. Lu, G. Wang, T. He, *Energy* **2018**, *150*, 759–769; b) C. Weng, Y. Cui, J. Sun, H. Peng, *J. Power Sources* **2013**, *235*, 36–44; c) X. Li, Z. Wang, J. Yan, *J. Power Sources* **2019**, *421*, 56–67; d) M. Dubarry, G. Baure, D. Anseán, *J. Electrochem. Energy Conversion Storage* **2020**, *17*, 044701.

[9] a) X. Li, Z. Wang, L. Zhang, C. Zou, D. D. Dorrell, *J. Power Sources* **2019**, *410*, 106–114; b) C. She, Z. Wang, F. Sun, P. Liu, L. Zhang, *IEEE Trans. Ind. Inform.* **2019**, *16*, 3345–3354; c) S. Zhang, X. Guo, X. Dou, X. Zhang, *J. Power Sources* **2020**, *479*, 228740.

[10] a) Y. Bao, W. Dong, D. Wang, *Energies* **2018**, *11*, 1073; b) C. Pastor-Fernández, K. Uddin, G. H. Chouchelamane, W. D. Widanage, J. Marco, *J. Power Sources* **2017**, *360*, 301–318.

[11] S. Jenu, A. Hentunen, J. Haavisto, M. Pihlatie, *J. Energy Storage* **2022**, *46*, 103855.

[12] Y. Jiang, J. Jiang, C. Zhang, W. Zhang, Y. Gao, N. Li, *J. Cleaner Prod.* **2018**, *205*, 754–762.

[13] D. Anseán, V. M. García, M. González, C. Blanco-Viejo, J. C. Viera, Y. F. Pulido, L. Sánchez, *IEEE Trans. Ind. Appl.* **2019**, *55*, 2992–3002.

[14] X. Tang, C. Zou, K. Yao, G. Chen, B. Liu, Z. He, F. Gao, *J. Power Sources* **2018**, *396*, 453–458.

[15] X. Lu, J. Qiu, G. Lei, J. Zhu, *IEEE Transactions on Transportation Electrification* **2023**, DOI: 10.1109/TTE.2023.3240617.

[16] N. Costa, L. Sanchez, D. Ansean, M. Dubarry, *J. Energy Storage* **2022**, *55*, 105558.

[17] K. A. Severson, P. M. Attia, N. Jin, N. Perkins, B. Jiang, Z. Yang, M. H. Chen, M. Aykol, P. K. Herring, D. Fraggedakis, *Nat. Energy* **2019**, *4*, 383–391.

[18] E. Kheirkhah-Rad, M. Moeini-Aghtaie, in *2021 31st Australasian Universities Power Engineering Conference (AUPEC)*, IEEE, **2021**, pp. 1–6.

[19] G. Ma, S. Xu, B. Jiang, C. Cheng, X. Yang, Y. Shen, T. Yang, Y. Huang, H. Ding, Y. Yuan, *Energy Environ. Sci.* **2022**, *15*, 4083–4094.

[20] M. Dubarry, V. Svoboda, R. Hwu, B. Y. Liaw, *Electrochem. Solid-State Lett.* **2006**, *9*, A454.

[21] a) C. She, L. Zhang, Z. Wang, F. Sun, P. Liu, C. Song, *IEEE Journal of Emerging and Selected Topics in Power Electronics* **2021**, *11*, 214–223, DOI: 10.1109/JESTPE.2021.3112754; b) Z. Xu, J. Wang, P. D. Lund, Y. Zhang, *Energy* **2021**, *225*, 120160.

[22] L. G. Brown, *ACM Comput. Surv.* **1992**, *24*, 325–376.

[23] R. Zhou, R. Zhu, C.-G. Huang, W. Peng, *J. Energy Storage* **2022**, *51*, 104560.

[24] E. Riviere, P. Venet, A. Sari, F. Meniere, Y. Bultel, in *2015 IEEE Vehicle Power and Propulsion Conference (VPPC)*, IEEE, **2015**, pp. 1–6.

[25] C. Weng, X. Feng, J. Sun, H. Peng, *Appl. Energy* **2016**, *180*, 360–368.

[26] H. Daumé, *A course in machine learning*, Hal Daumé III, **2017**.

[27] C. Cortes, V. Vapnik, *Machine learning* **1995**, *20*, 273–297.

[28] a) J. Kim, J. Yu, M. Kim, K. Kim, S. Han, *IFAC-PapersOnLine* **2018**, *51*, 392–397; b) X. Li, H. Jiang, S. Guo, J. Xu, M. Li, X. Liu, X. Zhang, *Comput. Intel. Neurosc.* **2022**, *2022*, DOI: 10.1155/2022/3920317.

[29] a) K. S. Mawonou, A. Eddahech, D. Dumur, D. Beauvois, E. Godoy, *J. Power Sources* **2021**, *484*, 229154; b) Y. Li, C. Zou, M. Berecibar, E. Nanini-Maury, J. C.-W. Chan, P. Van den Bossche, J. Van Mierlo, N. Omar, *Appl. Energy* **2018**, *232*, 197–210; c) Z. Chen, M. Sun, X. Shu, J. Shen, R. Xiao, in *2018 IEEE International Conference on Industrial Technology (ICIT)*, IEEE, **2018**, pp. 1754–1759.

[30] J. Brownlee, *Machine learning mastery with Python: understand your data, create accurate models, and work projects end-to-end*, Machine Learning Mastery, **2016**.